Uterine activin receptor-like kinase 5 is crucial for blastocyst implantation and placental development

Jia Peng[a,b,c], Diana Monsivais[a,c], Ran You[a], Hua Zhong[a], Stephanie A. Pangas[a,c,d], and Martin M. Matzuk[a,b,c,d,e,1]

[a]Department of Pathology and Immunology, Baylor College of Medicine, Houston, TX 77030; [b]Department of Molecular and Human Genetics, Baylor College of Medicine, Houston, TX 77030; [c]Center for Drug Discovery, Baylor College of Medicine, Houston, TX 77030; [d]Department of Molecular and Cellular Biology, Baylor College of Medicine, Houston, TX 77030; and [e]Department of Pharmacology, Baylor College of Medicine, Houston, TX 77030

Contributed by Martin M. Matzuk, July 23, 2015 (sent for review May 5, 2015; reviewed by Thomas E. Spencer and Haibin Wang)

Members of the transforming growth factor β (TGF-β) superfamily are key regulators in most developmental and physiological processes. However, the in vivo roles of TGF-β signaling in female reproduction remain uncertain. Activin receptor-like kinase 5 (ALK5) is the major type 1 receptor for the TGF-β subfamily. Absence of ALK5 leads to early embryonic lethality because of severe defects in vascular development. In this study, we conditionally ablated uterine ALK5 using progesterone receptor-cre mice to define the physiological roles of ALK5 in female reproduction. Despite normal ovarian functions and artificial decidualization in conditional knockout (cKO) mice, absence of uterine ALK5 resulted in substantially reduced female reproduction due to abnormalities observed at different stages of pregnancy, including implantation defects, disorganization of trophoblast cells, fewer uterine natural killer (uNK) cells, and impairment of spiral artery remodeling. In our microarray analysis, genes encoding proteins involved in cytokine–cytokine receptor interactions and NK cell-mediated cytotoxicity were down-regulated in cKO decidua compared with control decidua. Flow cytometry confirmed a 10-fold decrease in uNK cells in cKO versus control decidua. According to these data, we hypothesize that TGF-β acts on decidual cells via ALK5 to induce expression of other growth factors and cytokines, which are key regulators in luminal epithelium proliferation, trophoblast development, and uNK maturation during pregnancy. Our findings not only generate a mouse model to study TGF-β signaling in female reproduction but also shed light on the pathogenesis of many pregnancy complications in human, such as recurrent spontaneous abortion, preeclampsia, and intrauterine growth restriction.

TGF-β signaling | uterine luminal epithelium | trophoblast cells | uNK | female reproduction

The two crucial processes for the advancement of mammalian pregnancy are embryo implantation and formation of the placenta. When a blastocyst reaches the uterus, it includes two cell types, the inner cell mass, which later forms the embryo, and a layer of trophoblast, which later forms the placenta to facilitate nutrient uptake, waste elimination, and gas exchange between the embryo and the maternal uterus. In mice, the blastocyst reaches the uterus by 3.5 d postcoitum (dpc). There is only a limited time period for the uterus to support blastocyst implantation. At the beginning of the implantation widow, the closure of the uterine lumen results in closer contact between the luminal epithelium. After embryo attachment, the uterine stroma is transformed in preparation for trophoblast invasion in a process called decidualization. To achieve successful reproduction, a blastocyst competent for implantation needs to be synchronized with the proliferation and differentiation of specific uterine cell types under the control of two ovarian steroids, progesterone (P_4) and estradiol (E_2) (1, 2).

Murine placentation starts from the differentiation of trophectoderm (a layer of trophoblast in blastocyst). Mural trophectoderm develops to primary trophoblast giant cells. Meanwhile, polar trophectoderm becomes extraembryonic ectoderm and ectoplacental cone (EPC), which later give rise to labyrinth, spongiotrophoblasts, and secondary trophoblast giant cells. Thus, the mature placenta is composed of the outer maternal decidua, the middle junctional zone (including spongiotrophoblasts and trophoblast giant cells), and the innermost labyrinth (3). At midgestation, uterine natural killer (uNK) cells are the most abundant subset of lymphocytes found in implantation sites (4). In mice, a few uNK cells are first detected at 5 dpc, the onset of decidualization, and substantially increase in the decidua basalis until midgestation (5). To facilitate blood supply at the maternal–fetal interface during pregnancy, spiral artery remodeling begins around 9 dpc (6). This process involves thinning of the smooth muscle coat, enlarging of the luminal diameter, and reducing vessel resistance (7). By secreting cytokines and growth factors, uNK cells regulate gene expression in target tissues including vessel walls, endothelium, and uterine stroma (8). In addition, previous studies found that mice lacking interleukin 15 (IL-15) exhibit a reduced number of uNK cells and absence of decidual vessel modification in implantation sites, indicating that IL-15 is an essential cytokine required for uNK cell differentiation (9).

In mammals, members of the TGF-β superfamily are potent regulators of cell proliferation and differentiation in most developmental and physiological processes. Recent studies have defined the key roles of TGF-β signaling in multiple female reproductive events including ovarian folliculogenesis and ovulation (10–14), embryo implantation (15), uterine decidualization (15, 16), and placentation (17). Uterine-specific deletion of ligands and receptors in the TGF-β signaling pathway was facilitated by the generation of the progesterone receptor-cre (*PR-Cre*) mouse model (18). ALK5 is also known as the type 1 receptor for the TGF-β

Significance

Although many studies have yielded tremendous insights into the roles of TGF-β superfamily signaling pathways in physiological and pathophysiological processes, the in vivo roles of TGF-β signaling pathways in many aspects of reproduction remain largely unknown. To address these functions in females, we conditionally deleted the TGF-β type 1 receptor (activin receptor-like kinase 5, ALK5) and demonstrated that absence of TGF-β signaling through ALK5 in the uterus leads to striking abnormalities at different stages of pregnancy, including delayed implantation, disorganization of the trophoblast cells, significantly fewer uterine natural killer cells, and defects in spiral artery remodeling. Our findings provide a mouse model to investigate TGF-β signaling in reproduction and pave the way toward a better understanding of the pathogenesis of pregnancy-related complications in women.

Author contributions: J.P., S.A.P., and M.M.M. designed research; J.P., D.M., and R.Y. performed research; J.P., H.Z., and M.M.M. analyzed data; and J.P., D.M., S.A.P., and M.M.M. wrote the paper.

Reviewers: T.E.S., University of Missouri-Columbia; and H.W., Institute of Zoology, CAS.

The authors declare no conflict of interest.

[1]To whom correspondence should be addressed. Email: mmatzuk@bcm.edu.

This article contains supporting information online at www.pnas.org/lookup/suppl/doi:10.1073/pnas.1514498112/-/DCSupplemental.

www.pnas.org/cgi/doi/10.1073/pnas.1514498112

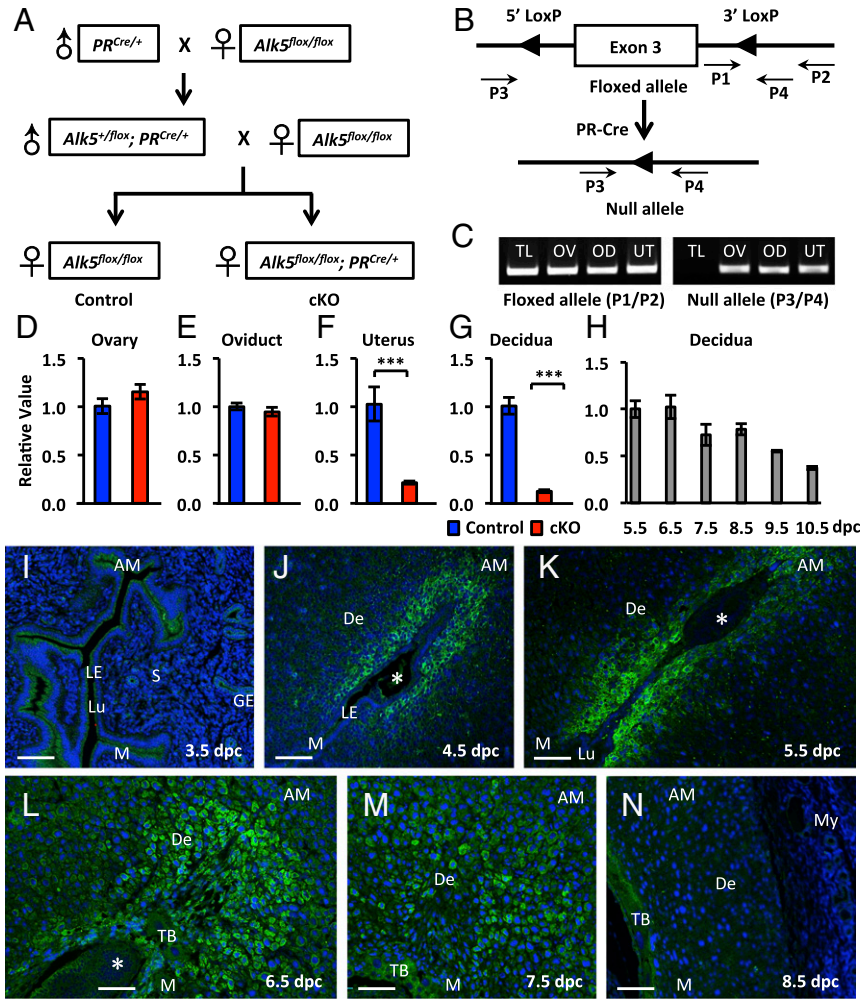

Fig. 1. Generation of the *Alk5* cKO female mice and expression of uterine ALK5. (*A*) Schematic representation of the breeding strategy to generate control and cKO females. (*B*) The *Alk5* null allele was generated by *PR-Cre*–mediated recombination. (*C*) PCR analysis for *Alk5* floxed and null alleles. OD, oviduct; OV, ovary; TL, tail; UT, uterus. (*D*–*G*) Relative *Alk5* mRNA levels in the ovary, oviduct, uterus, and 8.5 dpc decidua of control and cKO females. Data are presented as mean ± SEM ($n = 3$). $^{**}P < 0.01$; $^{***}P < 0.001$ compared with controls. (*H*) Relative *Alk5* mRNA levels measured by qPCR in wild-type decidua from 5.5 to 10.5 dpc. Data are presented as mean ± SEM ($n = 3$). (*I*–*N*) Expression and localization of uterine ALK5 were examined by immunofluorescence at sequential time points. Asterisk indicates an embryo. AM, antimesometrium; De, decidua; GE, glandular epithelium; LE, luminal epithelium; Lu, lumen; M, mesometrium; My, myometrium; S, stroma; TB, trophoblast. (Scale bar, 100 μm.)

subfamily, and *Alk5* null mice are embryonic lethal because of severe vascular defects (19). In this paper, we conditionally ablated uterine ALK5 to study its important roles during pregnancy. Deletion of uterine ALK5 led to multiple abnormalities during pregnancy including early implantation defects, disorganization of trophoblast cells, a significant reduction in the number of uNK cells, and impairment of spiral artery remodeling.

Results

Generation of *Alk5* cKO Mice and *Alk5* Expression in the Uterus. Because complete loss of ALK5 results in embryonic lethality (19), we generated an *Alk5* conditional knockout (cKO) mouse model using *PR-Cre* and an *Alk5* floxed allele in which exon 3 is flanked by *LoxP* sites (Fig. 1 *A* and *B*). Previous studies indicated that *PR-Cre* is expressed postnatally in the anterior lobe of pituitary glands, the corpus luteum, oviducts, and epithelial, stromal, and myometrial cellular compartments of uteri (18). To confirm *PR-Cre* mediated recombination in the female reproductive system, we performed PCR on DNA extracted from tails (as negative controls) and organs in the female reproductive tract of cKO mice (Fig. 1*C*). An *Alk5* floxed allele was detected in the tail, ovary, oviduct, and uterus, whereas an *Alk5* null allele was only detected in the female reproductive tract. Efficiency of *Alk5* deletion was further examined by real-time quantitative PCR (qPCR) to compare the mRNA levels among different organs (Fig. 1 *D*–*G*). qPCR primers were designed to detect the deleted exon 3 of *Alk5*. Significant reduction of the *Alk5* mRNA level was only detected in the uterus of virgin females as well as the decidua of pregnant females (Fig. 1 *F* and *G*), although *PR-Cre* was expressed in the entire female reproductive tract.

Previous studies have characterized the ALK5 expression pattern in the ovary, oviduct, and uterus by using an $Alk5^{\beta gal}$ knock-in allele (20). However, uterine ALK5 expression during pregnancy still remains unknown. Thus, we performed qPCR to measure decidual *Alk5* mRNA levels in the first half of gestation in wild type females (Fig. 1*H*). Decidual *Alk5* was highly expressed at 5.5 and 6.5 dpc, and then the mRNA levels gradually declined to 40% by 10.5 dpc. To further investigate the spatiotemporal localization of ALK5 in the uterus, we performed immunofluorescence analysis to trace ALK5 expression during sequential time points (Fig. 1 *I*–*N*). At 3.5 dpc, *Alk5* was weakly expressed in both luminal and glandular epithelial cells, but it was not detectable

Table 1. Six-month breeding trial with wild-type males

Genotype	Females	Pups	Litters	Pups/litter	Litters/female
Control	7	365	43	8.49 ± 0.31	6.14 ± 0.26
cKO	12*	9	3	3.00 ± 1.00	0.25 ± 0.13

*Five females died secondary to abnormal vaginal bleeding during pregnancy.

in stromal cells (Fig. 1*I*). When the embryo attaches to the uterine wall at 4.5 dpc, *Alk5* started to be expressed in the primary decidual zone at the antimesometrial (AM) pole (Fig. 1*J*). ALK5 expression extended to the decidual cells at the mesometrial (M) pole at 5.5 dpc (Fig. 1*K*) and was subsequently restricted to the AM decidua at 6.5 dpc (Fig. 1*L*). Consistent with the previous qPCR results, ALK5 protein levels gradually declined after 6.5 dpc (Fig. 1 *M* and *N*).

***Alk5* cKO Female Mice Exhibited Severe Defects in Fertility but Displayed Normal Histology of the Female Reproductive System.** To evaluate the fertility of *Alk5* cKO female mice, we performed a continuous breeding study for control and cKO female mice (Table 1). We mated 6-wk-old female mice ($n = 7$ for control and $n = 12$ for cKO) with known fertile wild-type male mice for 6 mo. The seven control females had normal breeding activity during the test period. In contrast, ablation of uterine *Alk5* led to sterility in 4 of the 12 females tested; 3 of the 12 females produced a total of 9 pups during the 6-mo breeding period, and the other 5 females died secondary to abnormal vaginal bleeding during pregnancy. Vaginal plugs were observed at similar frequencies between the two genotypes, which eliminated the possibility of abnormal mating behavior.

We investigated ovarian function to find out the possible cause of the severe fertility defects in the *Alk5* cKO females. In histological analyses, the *Alk5* cKO exhibited normal ovarian, oviductal, and nonpregnant uterine structures (Fig. S1 *A–H*), indicating that the severe fertility defects in *Alk5* cKO female mice were likely caused by uterine defects during pregnancy. Serum P_4 and E_2 levels were measured at different time points during pregnancy (Fig. S1 *I* and *J*). No significant variation of P_4 was detected between control and cKO female mice (Fig. S1*I*). The two groups exhibited comparable E_2 levels in early pregnancy, whereas the increase of E_2 with gestational age was slightly lower in the cKO female mice, suggesting lower E_2 production during placental development (Fig. S1*J*).

***Alk5* cKO Females Showed Extra Epithelial Folds and Luminal Closure Defects During Peri-Implantation.** Because there were no apparent defects in the reproductive tract of nonpregnant female mice, we next investigated the potential role of *Alk5* in early implantation. Embryo attachment leads to a local increase in capillary permeability, so implantation sites can be visualized at early stages by Chicago blue B dye injection (21). At 4.5 dpc, the cKO implantation sites were much smaller and faint blue compared with controls (Fig. 2*A*). One day later, the cKO implantation sites enlarged and became more visible with the injected dye (Fig. 2*B*). By 6.5 dpc, the size of the cKO implantation sites appeared comparable to controls (Fig. 2*C*).

During blastocyst attachment, uterine luminal closure occurs, resulting in formation of the implantation chamber (2). In our histological analysis, luminal closure was observed in control uterus at 4.5 dpc, which led to the closure of the uterine lumen with an AM–M axis (Fig. 2*D*). Meanwhile, incomplete luminal closure and extra epithelial folds were found in cKO uteri (Fig. 2*E*). At 5.5 dpc, the extra epithelial folds almost disappeared in cKO females (Fig. 2 *F* and *G*), and no obvious defect was observed by 6.5 dpc (Fig. 2 *H* and *I*). To further study the implantation defects in *Alk5* cKO mice, we examined prostaglandin-endoperoxide synthase 2 (PTGS2, an implantation marker) and cytokeratin 8 (CK8, an epithelial marker) protein expression and localization by immunofluorescence. PTGS2 has a dynamic localization correlating with different stages during implantation (22). At 4.5 dpc, PTGS2 was expressed in subepithelial stromal cells at the AM pole in controls (Fig. 2*J*). Besides the AM pole, PTGS2 was also localized around the extra epithelial fold in cKO implantation sites (Fig. 2*K*). At 5.5 dpc, PTGS2 shifted to decidual cells at the M pole in controls (Fig. 2*L*), but the shift of PTGS2 localization was delayed in cKO uteri, with PTGS2 remaining at the AM pole (Fig. 2*M*). At 6.5 dpc, PTGS2 was only visualized at the M pole in both control and cKO implantation sites (Fig. 2 *N* and *O*). Thus, the different expression pattern of PTGS2 in control and cKO suggested that lack of uterine ALK5 led to a delayed implantation.

Because the process of luminal closure during implantation is mainly controlled by P_4 and E_2 (2), we hypothesized that the lack of uterine lumen closure in *Alk5* cKO females resulted from an abnormal P_4 and/or E_2 response. To test this hypothesis, we first examined the uterine expression of *Esr1* (the gene encodes estrogen receptor α) and *Pgr* (the gene encodes PR) at 4.5 dpc. The mRNA levels of *Esr1* were significantly elevated in *Alk5* cKO females, whereas *Pgr* expression was comparable in the two genotypes (Fig. 2*P*). We tested another two E_2-responsive genes, *Muc1* and *Ltf* (23), and found their expression was significantly increased in *Alk5* cKO females (Fig. 2*P*). Several fibroblast growth factors (FGFs) have been previously reported to promote luminal epithelial proliferation via a paracrine manner (24), so we examined those FGF genes and found *Fgf18* was up-regulated in the *Alk5* cKO uteri (Fig. 2*P*). To characterize possible defects of initial decidualization during implantation, we tested two decidual marker genes, *Bmp2* and *Wnt4* (16, 25). *Bmp2* was significantly decreased in the cKO uteri, whereas *Wnt4* expression was similar in the two genotypes (Fig. 2*P*). We also performed immunohistochemical analysis to examine the expression of phosphorylated estrogen receptor α (pERα) and Ki67 (a proliferation marker) at 3.5 dpc. pERα was only detected in the stroma of control uterus (Fig. 2*Q*), but pERα-positive epithelial cells were also found in the cKO uterus (Fig. 2*R*). As we expected, Ki67 was only expressed in the stroma of control uterus (Fig. 2*S*), whereas *Alk5* cKO females highly expressed Ki67 in uterine epithelial cells (Fig. 2*T*). Collectively, these data indicate that the defective luminal closure and increased epithelial folding are likely associated with enhanced epithelial proliferation caused by increased uterine E_2 response during peri-implantation.

***Alk5* cKO Females Exhibited Fetal and Placental Abnormalities in Postimplantation.** To determine if there were defects later during pregnancy in *Alk5* cKO mice, we determined the number and weight of implantation sites from 7.5 to 10.5 dpc (Fig. 3 *A* and *B* and Fig. S2 *A–D*). At 7.5 dpc, implantation sites from the two groups showed similar numbers and normal weight. However, cKO females began to show fewer and smaller implantation sites at 8.5 dpc, and the differences between the two groups became more substantial over time. By 10.5 dpc, cKO implantation sites dropped to 60% in number and 50% in weight compared with controls. Furthermore, fetuses dissected from *Alk5* cKO females exhibited severe intrauterine growth restriction (IUGR) at 10.5 dpc (Fig. 3*C*). Because the fetuses are not mutants, conditional ablation of ALK5 in the maternal uterus led to the poor fetal growth.

To further characterize the uterine defects in postimplantation stages, we performed histological analysis of the implantation sites from 7.5 to 10.5 dpc (Fig. 3 *D–K* and Fig. S2 *E–L*). At 7.5 dpc, uterine decidualization, embryonic development, and extraembryonic structures appeared comparable between control and cKO females (Fig. 3 *D* and *E* and Fig. S2 *E* and *F*). Beginning at 8.5 dpc, hemorrhage and unclosed uterine lumens were observed in the cKO implantation sites (Fig. 3 *F* and *G*), concomitant with shallow

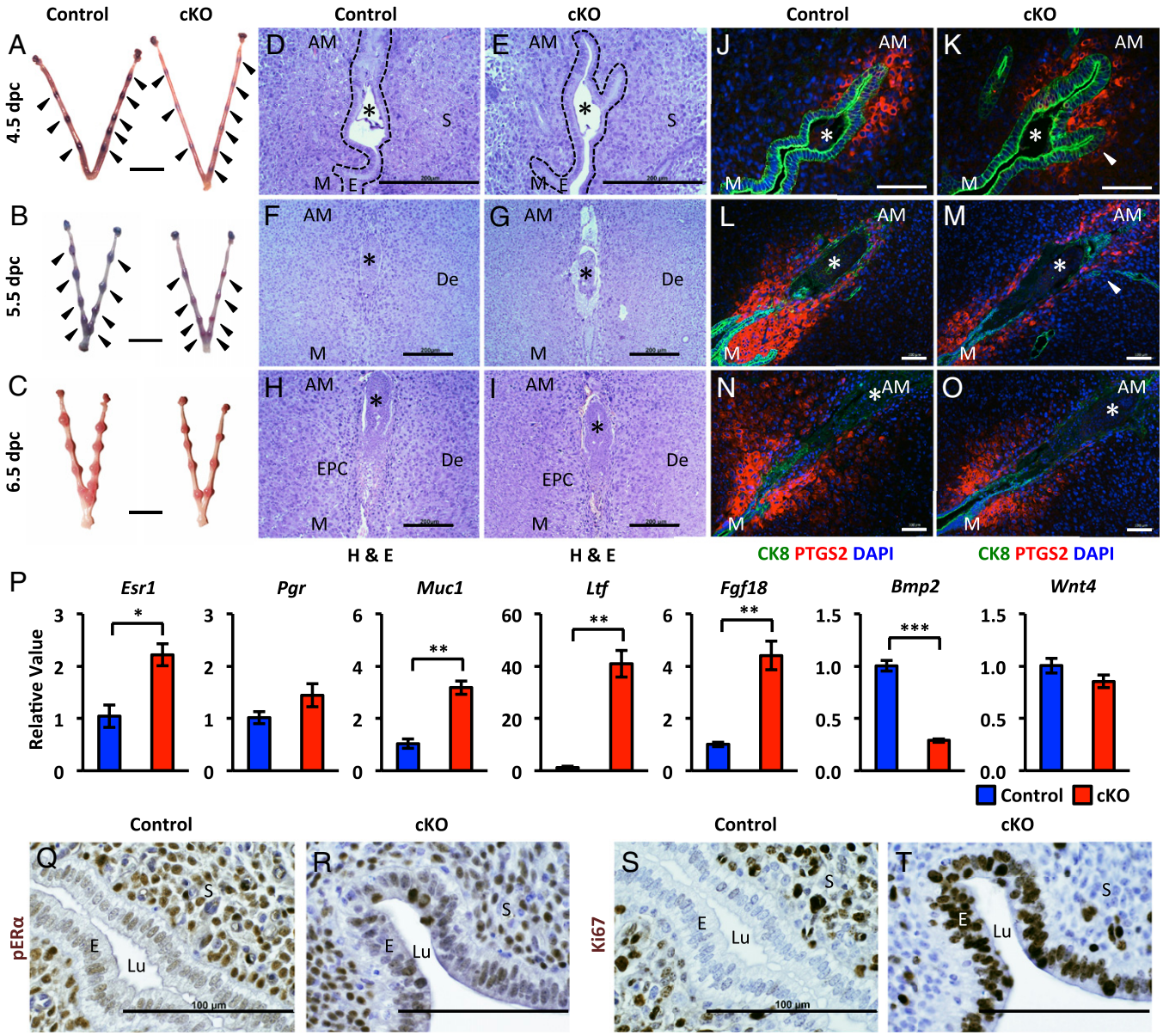

Fig. 2. *Alk5* cKO females showed defects during peri-implantation. (*A–C*) Gross morphology of control and cKO implantation sites. Chicago blue B dye was injected to the 4.5 and 5.5 dpc females. Early implantation sites were marked with black arrowheads. (Scale bar, 10 mm.) (*D–I*) H&E staining was performed to compare the histological differences between control and cKO females. (Scale bar, 200 μm.) (*J–O*) Immunofluorescence analysis of PTGS2 and CK8. (Scale bar, 100 μm.) (*P*) qPCR was performed to compare gene expression between control and cKO uteri at 4.5 dpc. Data are presented as mean ± SEM ($n = 5$). $^{*}P < 0.05$; $^{**}P < 0.01$; $^{***}P < 0.001$ compared with controls. (*Q–T*) Immunohistochemical analysis of pERα and Ki67 at 3.5 dpc. (Scale bar, 100 μm.) Asterisk indicates an embryo, white arrowhead indicates extra epithelial folds, and dashed line indicates luminal epithelium. AM, antimesometrium; De, decidua; E, epithelium; EPC, ectoplacental cone; Lu, lumen; M, mesometrium; S, stroma.

trophoblast invasion (Fig. S2 *G* and *H*). The hemorrhage was more extensive at 9.5 dpc, and we also observed a thicker AM uterine wall, which could restrict fetal growth (Fig. 3 *H* and *I* and Fig. S2 *I* and *J*). At 10.5 dpc, cKO females exhibited apparent abnormalities of the placenta, including expanded giant cells and an attenuated labyrinth layer (Fig. 3 *J* and *K* and Fig. S2 *K* and *L*).

Immunofluorescence analysis of PL-1 (a marker for trophoblast giant cells) and TPBPA (a marker for spongiotrophoblasts) was also performed to examine the critical role of ALK5 in postimplantation placentation (Fig. 3 *L–S*). No visible abnormalities were observed in the implantation sites at 7.5 dpc (Fig. 3 *L* and *M*), whereas *Alk5* cKO started to show shallow trophoblast invasion at 8.5 dpc (Fig. 3 *N* and *O*). TPBPA^{+} spongiotrophoblasts began to appear at 9.5 dpc in the two genotypes (Fig. 3 *P* and *Q*). At 10.5 dpc, controls had mature placentas with extended TPBPA^{+} spongiotrophoblast cells and a very thin layer of PL-1^{+} trophoblast giant cells (Fig. 3*R*). In addition to the labyrinth attenuation, fewer TPBPA^{+} spongiotrophoblasts were observed in the center of *Alk5* cKO placenta (Fig. 3*S*). The excessive trophoblast giant cells likely restricted the lateral extension of spongiotrophoblasts. Alternatively, it also could be secondary to more differentiated trophoblast giant cells at the expense of the TPBPA^{+} progenitor cells.

Deletion of Uterine ALK5 Resulted in Defects in uNK Cell Differentiation and Spiral Artery Remodeling. uNK cells are the most abundant types of immune cells at the maternal–fetal interface in early pregnancy (26). To investigate whether ALK5 is required for

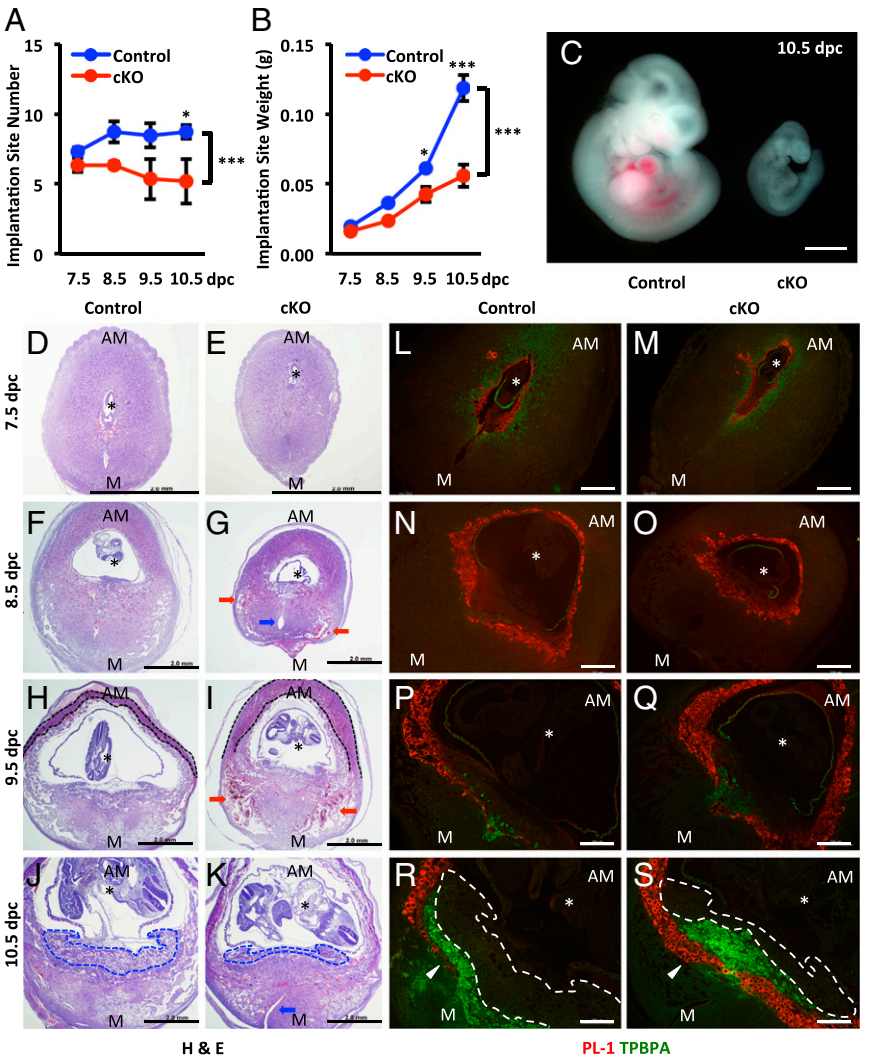

Fig. 3. Defects in decidualization and placentation were observed in the *Alk5* cKO females. (*A* and *B*) The number and weight of implantation sites were recorded from 7.5 to 10.5 dpc. Data are presented as mean ± SEM ($n = 5$). *$P < 0.05$; ***$P < 0.001$ compared with controls. (*C*) IUGR in the *Alk5* cKO uterus was observed at 10.5 dpc. (Scale bar, 1.0 mm.) (*D*–*K*) Histological analysis of implantation sites from 7.5 to 10.5 dpc. Blue arrow indicates unclosed uterine lumen, red arrow indicates hemorrhage, and blue dashed area indicates placental labyrinth. (Scale bar, 1.0 mm.) (*L*–*S*) Immunofluorescence analysis of PL-1 and TPBPA. (Scale bar, 500 μm.) Asterisk indicates embryo or fetus. AM, antimesometrium; M, mesometrium.

uNK recruitment and differentiation during decidualization, we used two well-established methods for detecting uNK cells, *Dolichos biflorus* agglutinin (DBA) and Periodic acid Schiff (PAS) staining (5, 27). Whereas a large number of DBA^+ uNK cells were detected in the control implantation sites by 9.5 dpc (Fig. 4 *A* and *C*), there were very few DBA^+ uNK cells in the cKO decidua basalis (Fig. 4 *B* and *D*). Similarly, many PAS^+ uNK cells with granules were present in the control implantation sites (Fig. 4*E*); PAS^+ uNK cells were almost absent in the decidua of *Alk5* cKO females (Fig. 4*F*). Thus, our data suggest that ALK5 is likely to be essential for precursor NK cell recruitment and uNK cell differentiation in the implantation sites.

Loss of uNK cells has been shown to cause structural abnormalities in pregnancy-induced modification of decidual arteries including smooth muscle thickening and luminal narrowing (8). To further establish the roles of ALK5 in spiral artery remodeling during placentation, we performed immunohistochemical analysis to examine the vascular defects with different molecular markers (Fig. 4 *G*–*N*). Upon staining for smooth muscle actin (SMA; a marker for smooth muscle cells within the vessel wall), we observed thinning and discontinuous smooth muscle cells of the arterial wall in controls (Fig. 4 *G* and *I*), indicating increased vessel permeability to facilitate nutrient exchange between fetus and mother. By contrast, thicker smooth muscle and smaller vessel lumen of uterine arteries were found in the cKO decidua basalis (Fig. 4 *H* and *J*). CD31 (a marker for endothelial cells) was used to confirm the lack of large vessels in *Alk5* cKO (Fig. 4 *K* and *L*). Furthermore, impaired formation of fetal blood vessels was also detected in cKO implantation sites by staining with laminin (a basement membrane marker) (Fig. 4 *O*–*R*).

Normal Artificial Decidualization but an Absence of uNK Cells Were Found in *Alk5* cKO Uteri. Uterine luminal closure defects were observed in *Alk5* cKO females, indicating possible impairment in decidualization. We artificially induced a decidual reaction to investigate roles of ALK5 in decidual cell proliferation and differentiation as well as to eliminate possible effects from the fetus (Fig. 5*A*). During artificial decidualization, one uterine horn is traumatized by a needle to mimic embryo attachment, and the other uterine horn is intact and serves as a control. Four days later, the decidual reaction is evaluated. As shown, both of the genotypes responded well to the mechanical stimulation (Fig. 5*B*),

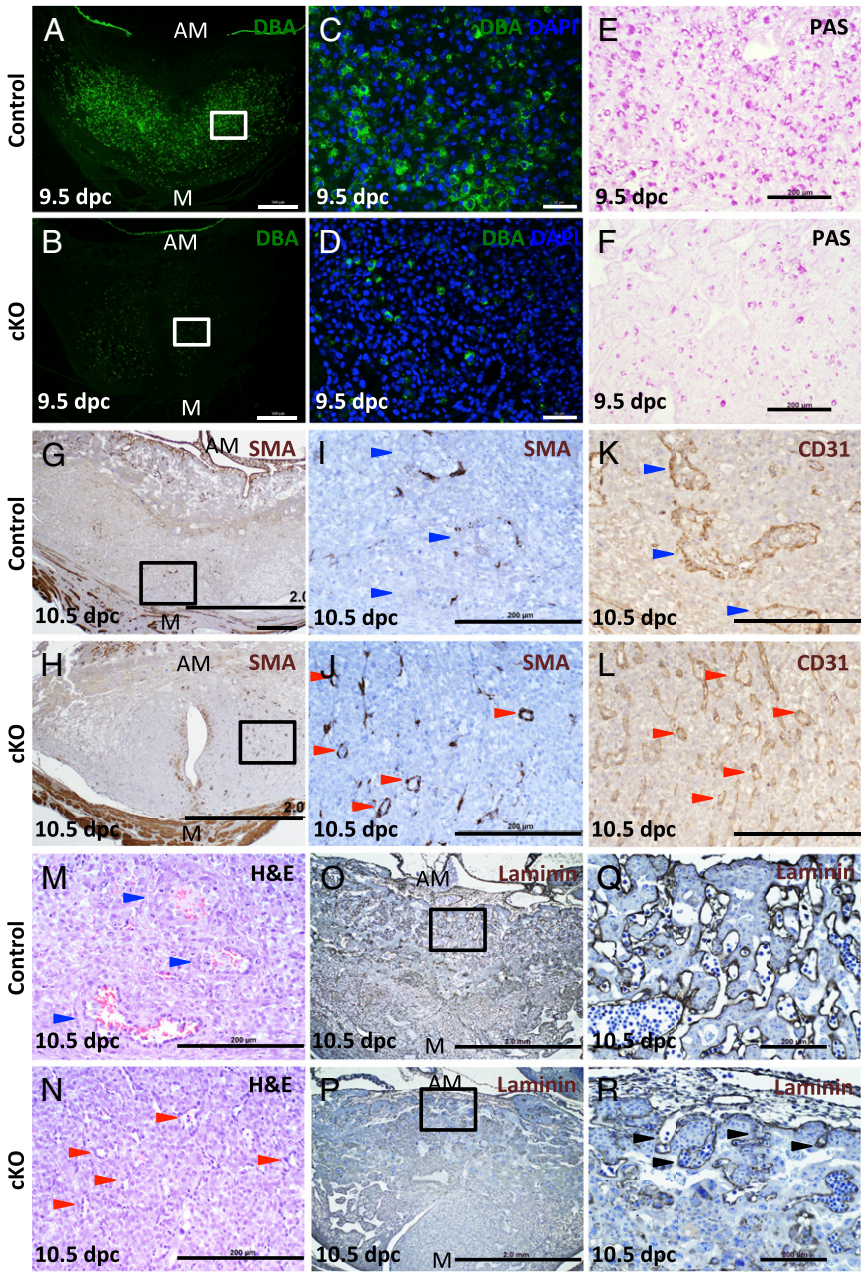

Fig. 4. The *Alk5* cKO female mice showed defects in uNK cell number and exhibited abnormalities in spiral artery remodeling. (*A*–*F*) DBA and PAS staining were performed to detect uNK cells in the M decidua. [Scale bar, 500 μm (*A* and *B*), 50 μm (*C* and *D*), and 200 μm (*E* and *F*).] (*G*–*N*) Defects in spiral artery remodeling were detected using immunohistochemistry and H&E staining. [Scale bar, 1.0 mm (*G* and *H*) and 200 μm (*I*–*N*).] Arrowhead indicates modified spiral artery in control (blue) or cKO (red) females. (*O*–*R*) Immunohistochemistry showed impaired formation of fetal blood vessels. Black arrowhead indicates fetal blood vessel in cKO females. [Scale bar, 2.0 mm (*O* and *P*) and 200 μm (*Q* and *R*).] AM, antimesometrium; M, mesometrium.

and there was no significant difference in uterine weight (Fig. 5*C*) or histological analysis (Fig. 5 *D*–*G*). Similar levels of Ki67 and alkaline phosphatase (ALP; a differentiation marker) were detected in the two genotypes (Fig. 5 *H*–*K*). Notably, uNK cells were almost absent in cKO decidua after artificial induction, indicating that the critical roles of ALK5 in uNK recruitment and maturation are independent of the defects observed in trophoblasts and embryos (Fig. 5 *L*–*G*).

uNK Deficiency in *Alk5* cKO Was Confirmed by Gene Expression Profiling and Flow Cytometry. To investigate the downstream pathways of TGF-β signaling via ALK5 during the decidualization process, we used microarrays to examine the gene expression profile in control and cKO decidua basalis collected at 8.5 dpc. As shown in the heat map, we found that the expression of 862 unique genes was significantly affected by the uterine deletion of *Alk5* (Fig. 6*A*). To extract biological insight from the 862 genes, we performed Gene Set Enrichment Analysis (GSEA) based on Kyoto Encyclopedia of Genes and Genomes (KEGG) gene sets and identified five main pathways (Fig. 6*B*). Of note, our data showed significant reduction in cytokine–cytokine receptor and NK cell-mediated cytotoxicity, which confirmed the reduced number of uNK cells and vascular abnormalities previously observed in the *Alk5* cKO mice. To better understand the biological importance of the five main pathways, we further grouped

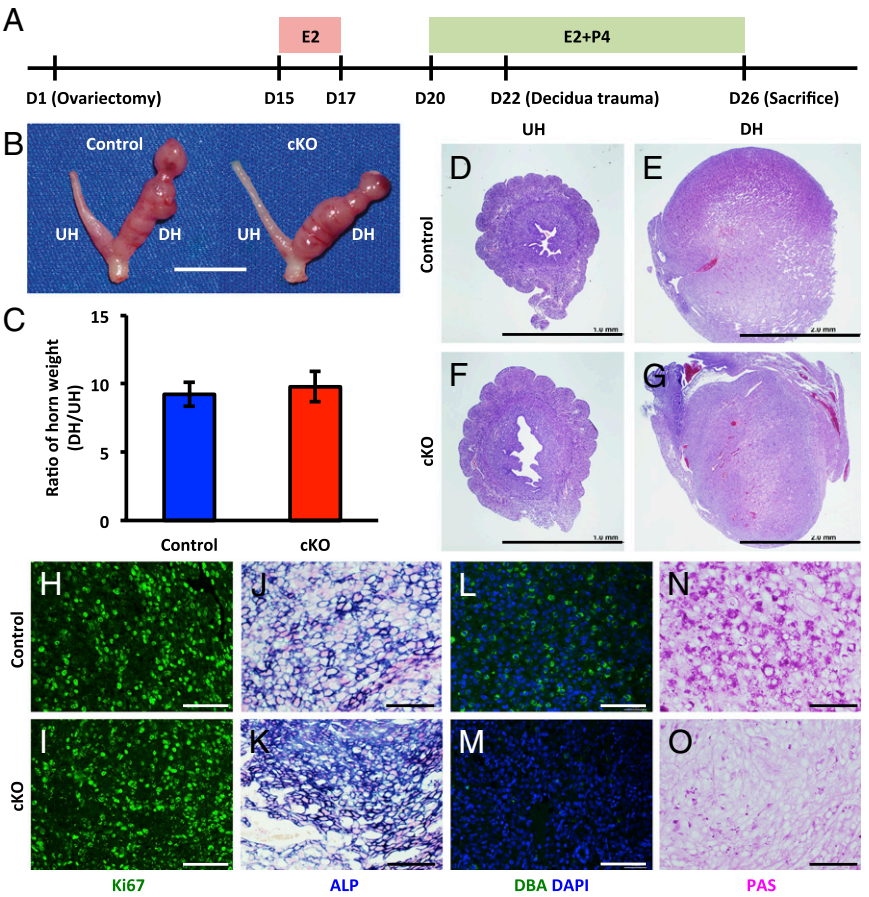

Fig. 5. Normal decidual proliferation and differentiation but an absence of uNK cells were found in artificially decidualized *Alk5* cKO females. (*A*) Representation of artificial decidualization procedures. (*B*) Gross morphology of uterine horns with or without stimulation. (Scale bar, 10 mm.) (*C*) Ratio of uterine horn weight between control and cKO. Data are presented as mean ± SEM ($n = 5$). (*D*–*G*) Histological analysis of uterine horn with or without stimulation. DH, decidulized horn; UH, unstimulated horn. [Scale bar, 1.0 mm (*D* and *F*) and 2.0 mm (*E* and *G*).] (*H*–*K*) Decidual proliferation and differentiation were examined by immunostaining of Ki67 and evaluation of endogenous ALP activity. (Scale bar, 100 μm.) (*L*–*O*) DBA and PAS staining were performed to detect uNK cells in the decidua of stimulated uterine horn. (Scale bar, 100 μm.)

leading edge subsets to show gene sets as core members of each pathway (Fig. 6*C*).

qPCR was performed to confirm the expression of genes involved in uNK maturation and spiral artery remodeling (Fig. 6*D*). mRNA levels of *Acta2*, the gene encoding SMA, were increased more than twofold in *Alk5* cKO decidua, indicating defects in the attenuation of the smooth muscle layer during vascular remodeling. IL-15 is a critical cytokine for NK cell differentiation (28). In *Alk5* cKO, *Il15* mRNA was substantially decreased, which explains the reduction of uNK during decidualization. As we expected, other NK-specific genes, including *Prf1* (29), *Klrg1* (30), *Nkg7* (31), and *CtsG* (32), and several granzyme genes (*GzmA*, *GzmB*, *GzmD*, *GzmE*, *GzmF*, and *GzmG*) (33) were significantly down-regulated in *Alk5* cKO decidua. Previous studies reported that CORIN (an atrial natriuretic peptide-converting enzyme) is essential for physiological changes at the maternal–fetal interface, and *Corin*-deficient mice mimic the features found in preeclampsia patients (34). Advillin (AVIL), an actin binding protein involved in cell morphogenesis (35), is located in uNK cells during decidualization (36). Herein, we observed that both *Corin* and *Avil* mRNA levels were substantially decreased in *ALK5* cKO females, suggesting the critical role of ALK5 in uNK maturation and spiral artery remodeling.

To further characterize and quantify the immune cell populations, we applied flow cytometry to compare the different leukocyte subsets including uNK cells, T cells, macrophages, and dendritic cells in both control and *Alk5* cKO decidua at 8.5 dpc (Fig. 6*E*). By gating cells that are DBA^+ cells but excluding $CD3^+$ cells, we observed that the DBA^+ $CD3^-$ uNK cells in *Alk5* cKO decidua were reduced to about 10% of the control decidua (Fig. 6 *F* and *G*). However, other types of leukocytes including T cells ($CD3^+$), macrophages, and dendritic cells ($CD11c^+$) were not significantly altered (Fig. 6*E*). Thus, uNK cells are the only leukocyte subset significantly decreased in *Alk5* cKO decidua compared with control decidua.

Discussion

In our current studies, we conditionally deleted uterine ALK5 and demonstrated that absence of TGF-β signaling through ALK5 leads to many abnormalities at different stages of pregnancy. One of the striking phenotypes was the reduction of uNK cells at midgestation. A previous study reported that mouse uNK cells do not express the PR (37). Thus, it is possible that TGF-βs (secreted from uterine epithelium or stroma, or even from the embryo) act on decidual cells via ALK5 to induce expression of other cytokines, which are key regulators in uNK cell maturation after embryo implantation. Among those cytokines that were down-regulated in *Alk5* cKO decidua, IL-15 has been previously reported as a key regulator in NK cell maturation (9). *Il15* null mice revealed complete absence of uNK cells as well as severe defects in spiral artery remodeling, which mimicked features observed in other uNK-deficient mouse models (9). Notably, *Il15*

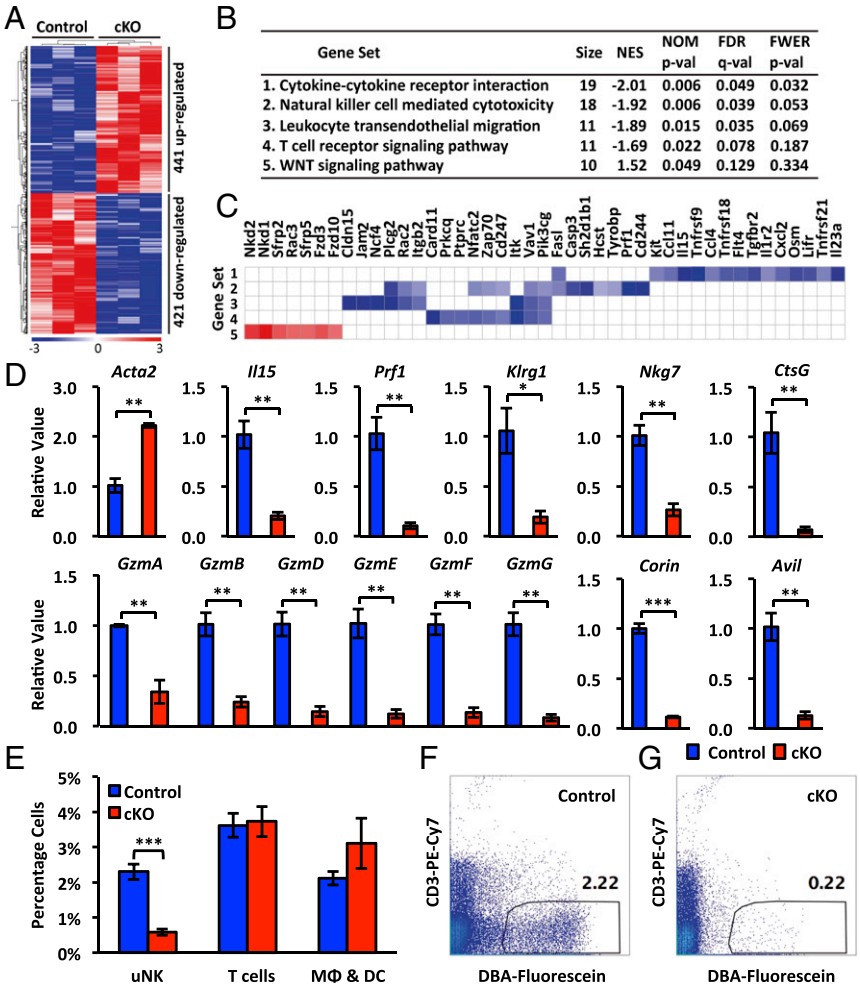

Fig. 6. Significantly altered gene expression in *Alk5* cKO decidua at 8.5 dpc. (*A*) Heat map showing hierarchical clustering of gene expression in control and *Alk5* cKO decidua. (*B*) Five KEGG biological pathways identified by GSEA. (*C*) The leading-edge subsets of the identified five gene sets. FDR q-val, false discovery rate; FWER p-val, family-wise error rate; NES, normalized enrichment score; NOM p-val, nominal *P* value. (*D*) qPCR was performed to compare gene expression between control and cKO decidua. Data are presented as mean ± SEM ($n = 5$). $^{*}P < 0.05$; $^{**}P < 0.01$; $^{***}P < 0.001$ compared with controls. (*E*) Flow cytometry was used to characterize different leukocyte subsets in control and cKO decidua. Data are presented as mean ± SEM ($n = 5$). $^{***}P < 0.001$ compared with controls. (*F* and *G*) uNK cells were identified as $DBA^{+}CD3^{-}$ cells and quantified in the leukocyte population. DC, dendritic cells; MΦ, macrophages.

mutants and our *Alk5* cKO shared very similar uterine gene expression profiles, particularly those genes specifically expressed in NK cells (e.g., *Prf1*, *Klrg1*, *Nkg7*, *CtsG*, and several granzyme genes) (36). However, no fetal loss was reported in either *Il15* null mutants or other NK cell-deficient mouse models (8, 9, 38, 39), indicating that reduction of uNK cells is not likely the main reason for the severe fertility defects that we observed in *Alk5* cKO females.

Several studies have reported that uNK cell-deficient mouse models exhibited no overgrowth of trophoblast or any consistent quantifiable impairment in fetus (6). Thus, the expansion of trophoblast giant cells and IUGR observed in our *Alk5* cKO mice are likely caused by other factors rather than absence of uNK cells at midgestation. Members of the TGF-β superfamily are grouped into two subfamilies according to their type 1 receptors as well as downstream SMAD pathways. TGF-βs, activins, and nodal phosphorylate SMAD2/3 via ALK4/5/7, whereas BMPs, most GDFs, and AMH phosphorylate SMAD1/5/8 via ALK2/3/6 (40). Our group previously described that conditional deletion of uterine BMPR2 (BMP type 2 receptor) led to female infertility due to abnormal vascular development, trophoblast defects, and absence of uNK cells (17). Those features are quite similar to the phenotypes we observed in *Alk5* cKO mice, indicating that BMP and TGF-β signaling play comparable but not redundant roles in placental development. Furthermore, our group found the expression pattern for the two proteins was quite different during early pregnancy. In the present study, ALK5 was highly expressed in the initial decidua surrounding the embryo, whereas BMPR2 significantly increases its expression in the M decidua at midgestation (17). In addition, low ALK5 expression remained in the AM decidua at midgestation, which did not colocalize with BMPR2 during placental development. According to the expression pattern of the two receptors, a possible explanation is that TGF-β (or other ligand) signaling via ALK5 might be required for earlier developmental events compared with BMP signaling via BMPR2 during pregnancy.

Although expression of TGF-βs and their receptors was previously implicated to play key roles during implantation (41), the molecular mechanism of this signaling pathway during early pregnancy remains poorly defined. As we described in the current study, early defects were also identified in our *Alk5* cKO females at 4.5 dpc, when blastocysts attached to the uterine wall, including extra epithelial folds and defective luminal closure. Interestingly, similar phenotypes have been recently reported in

multiple mouse models with excessive E_2 response during implantation (24, 42, 43). In mice, E_2 stimulates the proliferation of uterine epithelium on the first 2 d after conception, whereas the production of P_4 terminates the effects of E2 in epithelium growth from the third day. These hormone-regulated processes are required for preparing a receptive uterine environment for blastocyst attachment, which ensures successful reproduction (2, 44). However, the abnormally high E2 response observed in our *Alk5* cKO and other mouse models stimulates epithelial proliferation, prevents luminal closure, and results in impaired implantation (24, 42, 43). Although the early implantation defects found in *Alk5* cKO mice did not lead to complete failure of blastocyst implantation, it was likely associated with the maternal and fetal defects during later placentation, including trophoblast expansion, IUGR, uNK deficiency, and vascular abnormalities.

A full-term pregnancy in humans lasts about 40 wk without experiencing major health problems. However, the total rate of pregnancy loss after implantation is about 30% in healthy women (45). Most cases of failed pregnancy develop many complications, including recurrent spontaneous abortion, preeclampsia, IUGR, and preterm birth. Unfortunately, the physiological and pathological mechanisms of how those pregnancy complications develop in healthy mothers are still poorly understood. Because ethical issues are the major restrictions to the study of human pregnancy, animal models (and in particular mouse models) provide important insights into the molecular basis of human uterine physiology, pathology, and pregnancy complications. Herein, we successfully established a progressive mouse model mimicking multiple symptoms that appear at different stages of human pregnancy, such as implantation defects, trophoblast disorganization, IUGR, and vascular abnormalities due to uNK deficiency. Thus, our studies not only provide a mouse model to better understand how TGF-β signaling regulates female reproduction but also shed light on the pathogenesis of important reproductive health issues in human pregnancy, which can lead to the development of treatments for female infertility.

Materials and Methods

Animals. All mice used in this study were maintained on a mixed C57BL/6/129S6/SvEv genetic background and handled under protocols approved by the Institutional Animal Care and Use Committee at Baylor College of Medicine. Sequences of primers used for genotyping are listed in Table S1.

Histological Analysis. Tissues were dissected and fixed in 10% (vol/vol) neutral buffered formalin for 24 h and embedded in paraffin. Paraffin sections were stained with hematoxylin and eosin (H&E), PAS, or PAS–hematoxylin using standard procedures.

Immunohistochemistry and Immunofluorescence. Paraffin sections were deparaffinized, rehydrated, and boiled for antigen retrieval using standard procedures. After blocking with 3% (wt/vol) BSA for 1 h, sections were incubated with the primary antibodies overnight at 4 °C. Antibody information is listed in Table S2. Sections were incubated with biotinylated secondary antibodies and ABC reagent (Vector Laboratories), and immunoreactive signals were developed using a 3,3′-diaminobenzidine (DAB) substrate kit (Vector Laboratories). Immunofluorescence used a similar protocol except that the secondary antibodies were Alexa Fluor 488 or 594 (Life Technologies).

Hormone Analysis. Blood was collected from 2-mo-old adult female mice by cardiac puncture. The serum was separated from the blood and stored at −80 °C before the test. Serum P_4 and E_2 levels were measured in the Ligand Assay and Analysis Core at University of Virginia.

Artificial Induction of Decidualization. As previously described (46), 2-mo-old female mice were ovariectomized. After 2 wk, the mice were injected daily with 100 ng of E_2 for 3 d, followed by 2 d of rest. The mice were injected daily with 1 mg P_4 and 6.7 ng E_2 for 3 d. One uterine horn was scratched with a needle to artificially induce decidualization. As a control, the other uterine horn was not traumatized. The mice were continuously injected with P_4 and E_2 and progesterone for another 5 d. After sacrifice, both uterine horns were weighed, and the tissues were collected and fixed in 4% (wt/vol) paraformaldehyde for histological and immunohistochemical analysis.

RNA Isolation, qPCR, and Microarray Analysis. Total RNA was isolated using the RNeasy Mini kit (Qiagen). Gene expression was analyzed by qPCR with the SYBR Green detection system (Life Technologies). Primer information is listed in Table S3. The relative fold change of transcript was calculated by the $2^{-\Delta\Delta CT}$ method as described previously (47). For microarray analysis, the RNA samples were hybridized to Illumina Mouse WG-6 v.2.0 in the Microarray Core at University of Texas Health Science Center. Differentially expressed genes were defined by two-sided *t* test ($P < 0.05$) and fold change <0.5 and >2 and were displayed in a heat map using GenePattern (48). GSEA was performed based on KEGG gene sets, and gene sets that met the false discovery rate (FDR) < 0.25 criterion were chosen to further extract leading edge subsets (49).

Flow Cytometry. The decidua basalis were dissected from implantation sites, minced to small pieces, and then digested with 1 mg/mL collagenase IV and 0.2 mg/mL DNase I (Sigma-Aldrich) in HBSS for 45 min at 37 °C. Single cells were extracted by pipetting digested tissue and passed through a 40-μm cell strainer. Flow cytometry was performed with a BD LSR II (BD Biosciences) in the Cytometry and Cell Sorting Core at Baylor College of Medicine, and data were analyzed with FlowJo software (Tree Star Inc.). Forward scatter/side scatter gate was used to identify leukocyte populations as well as to eliminate debris. Antibodies (Table S2) were used to further identify different lymphocyte subsets.

Statistics. Comparison of means between two groups was conducted using *t* test. Two-way ANOVA was used to determine the differences between groups with respect to time and genotype. Data are presented as mean ± SEM, and $P < 0.05$ was considered to be statistically significant.

ACKNOWLEDGMENTS. We thank Dr. Stefan Karlsson for the gift of *Alk5* floxed mice and Drs. Francesco J. DeMayo and John P. Lydon for the gift of *PR-Cre* mice. These studies were supported by Eunice Kennedy Shriver National Institute of Child Health and Human Development Grants R01-HD33438 (to M.M.M.), R01-HD32067 (to M.M.M.), and R01-HD076980 (to S.A.P.) and National Cancer Institute Grant R01-CA138628 (to S.A.P.).

1. Paria BC, Reese J, Das SK, Dey SK (2002) Deciphering the cross-talk of implantation: Advances and challenges. *Science* 296(5576):2185–2188.
2. Wang H, Dey SK (2006) Roadmap to embryo implantation: Clues from mouse models. *Nat Rev Genet* 7(3):185–199.
3. Watson ED, Cross JC (2005) Development of structures and transport functions in the mouse placenta. *Physiology (Bethesda)* 20:180–193.
4. Moffett-King A (2002) Natural killer cells and pregnancy. *Nat Rev Immunol* 2(9):656–663.
5. Paffaro VA, Jr, Bizinotto MC, Joazeiro PP, Yamada AT (2003) Subset classification of mouse uterine natural killer cells by DBA lectin reactivity. *Placenta* 24(5):479–488.
6. Greenwood JD, et al. (2000) Ultrastructural studies of implantation sites from mice deficient in uterine natural killer cells. *Placenta* 21(7):693–702.
7. Croy BA, et al. (2003) Uterine natural killer cells: Insights into their cellular and molecular biology from mouse modelling. *Reproduction* 126(2):149–160.
8. Ashkar AA, Di Santo JP, Croy BA (2000) Interferon gamma contributes to initiation of uterine vascular modification, decidual integrity, and uterine natural killer cell maturation during normal murine pregnancy. *J Exp Med* 192(2):259–270.
9. Ashkar AA, et al. (2003) Assessment of requirements for IL-15 and IFN regulatory factors in uterine NK cell differentiation and function during pregnancy. *J Immunol* 171(6):2937–2944.
10. Matzuk MM, Kumar TR, Bradley A (1995) Different phenotypes for mice deficient in either activins or activin receptor type II. *Nature* 374(6520):356–360.
11. Dong J, et al. (1996) Growth differentiation factor-9 is required during early ovarian folliculogenesis. *Nature* 383(6600):531–535.
12. Elvin JA, Clark AT, Wang P, Wolfman NM, Matzuk MM (1999) Paracrine actions of growth differentiation factor-9 in the mammalian ovary. *Mol Endocrinol* 13(6):1035–1048.
13. Brown CW, Houston-Hawkins DE, Woodruff TK, Matzuk MM (2000) Insertion of Inhbb into the Inhba locus rescues the Inhba-null phenotype and reveals new activin functions. *Nat Genet* 25(4):453–457.
14. Jorgez CJ, Klysik M, Jamin SP, Behringer RR, Matzuk MM (2004) Granulosa cell-specific inactivation of follistatin causes female fertility defects. *Mol Endocrinol* 18(4):953–967.
15. Clementi C, et al. (2013) Activin-like kinase 2 functions in peri-implantation uterine signaling in mice and humans. *PLoS Genet* 9(11):e1003863.
16. Lee KY, et al. (2007) Bmp2 is critical for the murine uterine decidual response. *Mol Cell Biol* 27(15):5468–5478.
17. Nagashima T, et al. (2013) BMPR2 is required for postimplantation uterine function and pregnancy maintenance. *J Clin Invest* 123(6):2539–2550.

18. Soyal SM, et al. (2005) Cre-mediated recombination in cell lineages that express the progesterone receptor. *Genesis* 41(2):58–66.
19. Larsson J, et al. (2001) Abnormal angiogenesis but intact hematopoietic potential in TGF-beta type I receptor-deficient mice. *EMBO J* 20(7):1663–1673.
20. Li Q, et al. (2011) Transforming growth factor β receptor type 1 is essential for female reproductive tract integrity and function. *PLoS Genet* 7(10):e1002320.
21. Paria BC, Huet-Hudson YM, Dey SK (1993) Blastocyst's state of activity determines the "window" of implantation in the receptive mouse uterus. *Proc Natl Acad Sci USA* 90(21):10159–10162.
22. Chakraborty I, Das SK, Wang J, Dey SK (1996) Developmental expression of the cyclo-oxygenase-1 and cyclo-oxygenase-2 genes in the peri-implantation mouse uterus and their differential regulation by the blastocyst and ovarian steroids. *J Mol Endocrinol* 16(2):107–122.
23. Gibson MK, et al. (1991) The mechanism of ICI 164,384 antiestrogenicity involves rapid loss of estrogen receptor in uterine tissue. *Endocrinology* 129(4):2000–2010.
24. Li Q, et al. (2011) The antiproliferative action of progesterone in uterine epithelium is mediated by Hand2. *Science* 331(6019):912–916.
25. Franco HL, et al. (2011) WNT4 is a key regulator of normal postnatal uterine development and progesterone signaling during embryo implantation and decidualization in the mouse. *FASEB J* 25(4):1176–1187.
26. Croy BA, Kiso Y (1993) Granulated metrial gland cells: A natural killer cell subset of the pregnant murine uterus. *Microsc Res Tech* 25(3):189–200.
27. Peel S (1989) Granulated metrial gland cells. *Adv Anat Embryol Cell Biol* 115:1–112.
28. Kennedy MK, et al. (2000) Reversible defects in natural killer and memory CD8 T cell lineages in interleukin 15-deficient mice. *J Exp Med* 191(5):771–780.
29. Parr EL, Young LH, Parr MB, Young JD (1990) Granulated metrial gland cells of pregnant mouse uterus are natural killer-like cells that contain perforin and serine esterases. *J Immunol* 145(7):2365–2372.
30. Li Y, et al. (2009) Structure of natural killer cell receptor KLRG1 bound to E-cadherin reveals basis for MHC-independent missing self recognition. *Immunity* 31(1):35–46.
31. Turman MA, Yabe T, McSherry C, Bach FH, Houchins JP (1993) Characterization of a novel gene (NKG7) on human chromosome 19 that is expressed in natural killer cells and T cells. *Hum Immunol* 36(1):34–40.
32. Croy BA, et al. (2010) Analysis of uterine natural killer cells in mice. *Methods Mol Biol* 612:465–503.
33. Allen MP, Nilsen-Hamilton M (1998) Granzymes D, E, F, and G are regulated through pregnancy and by IL-2 and IL-15 in granulated metrial gland cells. *J Immunol* 161(6): 2772–2779.
34. Cui Y, et al. (2012) Role of corin in trophoblast invasion and uterine spiral artery remodelling in pregnancy. *Nature* 484(7393):246–250.
35. Shibata M, et al. (2004) Type F scavenger receptor SREC-I interacts with advillin, a member of the gelsolin/villin family, and induces neurite-like outgrowth. *J Biol Chem* 279(38):40084–40090.
36. Bany BM, Scott CA, Eckstrum KS (2012) Analysis of uterine gene expression in interleukin-15 knockout mice reveals uterine natural killer cells do not play a major role in decidualization and associated angiogenesis. *Reproduction* 143(3):359–375.
37. Oh MJ, Croy BA (2008) A map of relationships between uterine natural killer cells and progesterone receptor expressing cells during mouse pregnancy. *Placenta* 29(4): 317–323.
38. Barber EM, Pollard JW (2003) The uterine NK cell population requires IL-15 but these cells are not required for pregnancy nor the resolution of a Listeria monocytogenes infection. *J Immunol* 171(1):37–46.
39. Kim S, Iizuka K, Aguila HL, Weissman IL, Yokoyama WM (2000) In vivo natural killer cell activities revealed by natural killer cell-deficient mice. *Proc Natl Acad Sci USA* 97(6):2731–2736.
40. Miyazawa K, Shinozaki M, Hara T, Furuya T, Miyazono K (2002) Two major Smad pathways in TGF-beta superfamily signalling. *Genes Cells* 7(12):1191–1204.
41. Roelen BA, Lin HY, Knezević V, Freund E, Mummery CL (1994) Expression of TGF-beta s and their receptors during implantation and organogenesis of the mouse embryo. *Dev Biol* 166(2):716–728.
42. Daikoku T, et al. (2011) Conditional deletion of Msx homeobox genes in the uterus inhibits blastocyst implantation by altering uterine receptivity. *Dev Cell* 21(6): 1014–1025.
43. Zhang S, et al. (2014) Uterine Rbpj is required for embryonic-uterine orientation and decidual remodeling via Notch pathway-independent and -dependent mechanisms. *Cell Res* 24(8):925–942.
44. Dey SK, et al. (2004) Molecular cues to implantation. *Endocr Rev* 25(3):341–373.
45. Wilcox AJ, et al. (1988) Incidence of early loss of pregnancy. *N Engl J Med* 319(4): 189–194.
46. Lee K, et al. (2006) Indian hedgehog is a major mediator of progesterone signaling in the mouse uterus. *Nat Genet* 38(10):1204–1209.
47. Livak KJ, Schmittgen TD (2001) Analysis of relative gene expression data using real-time quantitative PCR and the 2(-Delta Delta C(T)) method. *Methods* 25(4):402–408.
48. Reich M, et al. (2006) GenePattern 2.0. *Nat Genet* 38(5):500–501.
49. Subramanian A, et al. (2005) Gene set enrichment analysis: A knowledge-based approach for interpreting genome-wide expression profiles. *Proc Natl Acad Sci USA* 102(43):15545–15550.